

dc-GAN: Dual-Conditioned GAN for Face Demorphing From a Single Morph

Nitish Shukla
Michigan State University
shuklan3@msu.edu

Arun Ross
Michigan State University
rossarun@msu.edu

Abstract

A facial morph is an image strategically created by combining two face images pertaining to two distinct identities. The goal is to create a face image that can be matched to two different identities by a face matcher. Face demorphing inverts the process and tries to recover the original images constituting a facial morph. Existing demorphing techniques are either very restrictive (assume identities during testing) or produce feeble outputs (both outputs look very similar - the morph-replication problem). In this paper, we overcome these issues by proposing dc-GAN (dual-conditioned GAN), a novel demorphing method conditioned on the morph image as well as the embedding extracted from the image. Our method overcomes morph-replication and produces high quality reconstructions of the bonafide images used to create the morphs. Moreover, our method is highly generalizable across demorphing paradigms (differential/reference-free). We conduct experiments on AMSL, FRLL-Morphs and MorDiff datasets to showcase the efficacy of our method. Code and train-test split are available at hidden for blind review.

1. Introduction

Morphing, in the biometric literature, refers to the blending of two or more face images to generate a composite image that matches the identities of the images used to create it. This matching is with respect to an automated Face Recognition System (FRS). Such a composite image, known as a facial morph, can be incorporated into a biometric-based identity document thereby allowing multiple individuals to use the same document. This can compromise national security [23, 25]. Historically, morphs were created by extracting facial landmarks from face images and then combining the two face images [1, 14, 31]. However, more recently, deep learning models have been remarkably successful in generating high-quality morphs, especially, those based on generative paradigms like diffu-

sion models [7] and generative adversarial attacks [4, 8, 12].

Morph Attack Detection (MAD) is essential for retaining the integrity, security and reliability of a biometric system. Current MAD techniques can be broadly divided into two categories: i) reference-based differential-image technique [13, 34], and ii) reference-free single-image techniques [2, 5, 38]. Reference-based methods have two images: the input face image (say, on the passport) and a reference face image (say, the live image of a person acquired at the port of entry). Reference-free methods have only one image: the input face image. While MAD techniques can reliably flag facial morphs, they do not reveal the images involved in the creation of the morph. From a forensic standpoint, it is valuable to recover images of the constituent identities¹ from a morph flagged by an MAD software. This process of extracting constituent face images from a morph image is called face demorphing. Limited work exists in this field, especially in the reference-free category. In this paper, we focus on both reference-based as well as reference-free face demorphing. To set up the problem, we first identify multiple scenarios that are plausible in the real world. In the context of this work, the choice of train and test data will define these scenarios. To formally define the various scenarios arising in real life, let \mathcal{X}_{train} , \mathcal{Y}_{train} denote the training data corresponding to the morphs and bonafides, respectively. Assume that all morph images in \mathcal{X}_{train} images are necessarily generated only using the identities in \mathcal{Y}_{train} .

$$\forall x \in \mathcal{X}_{train}, \mathcal{M}(y_1, y_2) = x \Rightarrow \{y_1, y_2\} \in \mathcal{Y}_{train} \quad (1)$$

where, \mathcal{M} is the morphing operator. Test sets \mathcal{X}_{test} , \mathcal{Y}_{test} are defined similarly. We now define three scenarios: i) Train and test morphs are obtained from the same pool of identities. ii) Some train and test morphs share the same identities but not all. iii) Train and test morphs are generated from a disjoint pool of identities. These conditions can be

¹The constituent images are referred to as “bonafides” since in some literature, they are real images of real people.

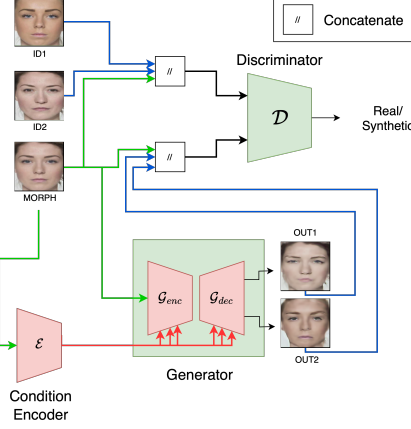


Figure 1. Dual-Conditioned GAN for Reference-Free Demorphing: An image encoder, \mathcal{E} , encodes the morph image, which is then used as a condition in the generator. The generator, based on a UNet architecture, \mathcal{G} , takes in the MORPH image and the encoded representation, $\mathcal{E}(\text{MORPH})$, producing two outputs, OUT1 and OUT2. The discriminator is trained to distinguish between the real set (MORPH, BF1, BF2) and the synthetic set (MORPH, OUT1, OUT2), differentiating real from synthetic pairs.

formally defined as:

- Scenario 1) $\mathcal{Y}_{test} \subseteq \mathcal{Y}_{train}, \mathcal{X}_{train} \cap \mathcal{X}_{test} = \phi$
- Scenario 2) $\mathcal{Y}_{test} \subset \mathcal{Y}_{train}, \mathcal{X}_{train} \cap \mathcal{X}_{test} = \phi$ (2)
- Scenario 3) $\mathcal{Y}_{test} \cap \mathcal{Y}_{train} = \mathcal{X}_{train} \cap \mathcal{X}_{test} = \phi$

Most of the previous work assumed scenario 1 implicitly [38, 39], but this is a strong assumption hampering the generalisability of the demorphing technique. Limited research has been conducted on demorphing in scenario 3, and most techniques seem to merely replicate the morph in both the outputs [5].

In this work, we propose a demorphing technique free of any assumption regarding the identities of images (scenario 3) and can be used for both reference-based and reference-free demorphing. .

In summary, our contributions are as follows:

- We propose dc-GAN, a novel GAN-based technique designed to extract constituent images from a single morph. Our approach is well-suited for both reference-free and differential demorphing tasks.
- We conduct a thorough analysis of the *implicit bias* present in morphs and extensively benchmark publicly available face recognition systems (FRS) on demorphing tasks in the presence of high frequency visible artefacts which arise during demorphing process.
- To the best of our knowledge, our method is the first to overcome the issue of *morph-replication* on unseen identities (scenario 3).

2. Background

Face morphing refers to the process of combining two or more face images corresponding to two distinct identities to produce another face image (called a morph) which has a high biometric similarity (or lower distance), as assessed by an automated face matcher. Typically, a morphing operator, \mathcal{M} , acts upon two input bonafides, \mathcal{I}_1 and \mathcal{I}_2 , to produce the morph \mathcal{X} :

$$\mathcal{X} = \mathcal{M}(\mathcal{I}_1, \mathcal{I}_2) \quad (3)$$

The goal of \mathcal{M} is to ensure that $\mathcal{B}(\mathcal{I}_1, \mathcal{X}) > \tau$ and $\mathcal{B}(\mathcal{I}_2, \mathcal{X}) > \tau$ where \mathcal{B} is a biometric face matcher that produces a similarity score and τ is the similarity threshold.

Face demorphing is the inverse of the morphing process. Given a morph \mathcal{X} , the goal is to recover the face images used to produce \mathcal{X} . Initial work on demorphing were primarily reference-based, i.e., they required an image of one of the identities to recover the other [6, 13]. The authors also assumed prior knowledge about the morphing factor used during the morphing process. FD-GAN [28] is a reference-based method which uses a symmetric GAN architecture and attempts to recover an image of the first identity from the morphed input using an image of the second identity. To validate the effectiveness of its generative model, it then tries to recover the second identity using the output of the first identity. More recently, reference-free demorphing techniques have also been proposed with some degree of success. In [5], the authors decompose the morph image into two output images using a GAN that is composed of a generator, a decomposition critic, and two Markovian discriminators. Shukla [38] proposed a diffusion-based method for scenario 1 that iteratively adds noise to the morph image and recovers the constituent face images during the backward process. In [39], the authors decompose the morph into multiple privacy-preserving components using an encoder, and then recover the constituent face images by weighting and combining these components with a decoder.

3. Proposed Method

Face demorphing is the inverse of the morphing problem. The intricacy lies not only in the absence of the morphing technique used (landmark-based or deep learning based) but also in the lack of constraints on the output space. Given a morph \mathcal{X} , the goal of the demorphing operator, denoted as \mathcal{DM} is to recover the constituent face images,

$$\mathcal{O}_1, \mathcal{O}_2 = \mathcal{DM}(\mathcal{X}) \quad (4)$$

satisfying the following conditions:

$$||\mathcal{B}(\mathcal{O}_1) - \mathcal{B}(\mathcal{O}_2)||^2 < \theta \quad (5)$$

and,

$$\max_{j \in \{1,2\}} \max_{\substack{k \in \{1,2\} \\ k \neq j}} (||\mathcal{B}(O_j) - \mathcal{B}(I_k)||^2, ||\mathcal{B}(O_j) - \mathcal{B}(I_j)||^2) > \epsilon \quad (6)$$

where θ and ϵ are similarity thresholds. Equation 5 enforces the reconstructed outputs to look dissimilar among themselves, an issue referred to as morph replication, while Equation 6 enforces that each output aligns with its corresponding ground truth image.

In [5], the authors attempt to recover identities from a single image using a GAN [15] that includes a generator for demorphing and three Markovian discriminators. However, the method has a limitation, where the outputs not only closely resemble the morph image but also appear similar to each other. We term this phenomenon as *morph-replication*. This issue arises because the morphing operator \mathcal{M} is a highly nonlinear function, making demorphing an ill-posed problem. Although their method employs three discriminators to optimize output similarity and visual realism, the generator only receives the morph image, which provides insufficient guidance for the demorphing process. The morph image alone may not be adequate to recover both constituent face images.

Inspired by their work, our method also utilizes GAN, but with a key difference: we introduce conditioning on both the generator and discriminator. This conditioning provides more robust guidance for the generation of constituent images. We illustrate the architecture of our method in Figure 1. A UNet [33] generator \mathcal{G} , based on an encoder-decoder architecture receives the morph input and generates two outputs. Simultaneously, an image encoder \mathcal{E} encodes the morph image and feeds the resulting embedding into the generator. This morph embedding is injected into the intermediate latent layers of the generator. We refer to our method as a dual-conditioned GAN (dc-GAN), conditioned on (i) the morph image in the image domain and (ii) morph image embeddings in the latent domain. The discriminator receives a “real” triplet, consisting of the morph image along with the ground truth images, and a “fake” triplet, composed of the morph image and the two generated outputs. The discriminator is then trained in an adversarial fashion alongside the generator to distinguish the real triplet from the synthetically generated one. Note that we also condition the discriminator with the morph image, providing it with the context needed to distinguish the morph from the constituent ground-truth images. The conditions work in tandem to ensure that morph-replication does not occur.

For differential, i.e., reference-based demorphing, we modify our pipeline slightly. The image encoder now encodes both the morph image and the reference image, concatenating them to provide guidance for the generator. The generator receives both the morph and reference images as input (with 6 channels) and outputs the reconstructed image

(with 3 channels corresponding to RGB). The discriminator architecture and function remain unchanged.

3.1. Loss Functions

The loss function for dc-GAN can be expressed as:

$$\min_{\mathcal{G}} \max_{\mathcal{D}} \mathcal{L}_{\text{dcGAN}}(\mathcal{D}, \mathcal{G}) = \mathbb{E}_{(x,y) \sim p_{\text{data}}(\cdot)} [\log \mathcal{D}(\mathbf{y}|x)] + \mathbb{E}_{z \sim p_z(z), (x,y) \sim p_{\text{data}}(\cdot)} [\log(1 - \mathcal{D}(\mathcal{G}(z|x, \mathcal{E}(x))|x))] \quad (7)$$

The generator is conditioned on the morph, x , and its representation, $\mathcal{E}(x)$. We denote the bonafide image-pairs as \mathbf{y} . Similarly, the discriminator is conditioned on the morph as well. We introduce noise exclusively through dropout, which is applied to several layers of our generator during both training and test phases, following the approach suggested in [18].

However, previous approaches observed that generating face images without explicit guidance results in blurry and less discriminatory features [27]. On this account, we add another component to the loss function, along with the standard dc-GAN loss, which guides the model to generate feature-rich faces. Another issue is the lack of order in the generator’s outputs (outputs are generated in no specific order). To address this, we align the generator’s outputs with the ground-truth face images using the widely-employed cross-road loss [5].

$$\mathcal{L}_{cr} = \begin{cases} \min[\mathcal{L}_1(\mathcal{I}_1, \mathcal{O}_1) + \mathcal{L}_1(\mathcal{I}_2, \mathcal{O}_2), \\ \mathcal{L}_1(\mathcal{I}_1, \mathcal{O}_2) + \mathcal{L}_1(\mathcal{I}_2, \mathcal{O}_1)] & \text{if reference free} \\ \mathcal{L}_1(\mathcal{I}, \mathcal{O}) & \text{if differential} \end{cases} \quad (8)$$

where, \mathcal{L}_1 is the standard per-pixel loss, $\{\mathcal{I}_1, \mathcal{I}_2\}$ are the ground-truth face images and $\{\mathcal{O}_1, \mathcal{O}_2\}$ are the generated outputs from our method. In the case of reference-free demorphing from a single morph, the model generates two images, which are compared against the two ground-truth face images. The cross-road loss matches the correct output to the ground truth by computing the \mathcal{L}_1 loss between all possible pairs (only two). Taking the minimum ensures that the correct match is selected. For differential demorphing, the cross-road loss simplifies to the \mathcal{L}_1 loss between the single output \mathcal{O} , and the single ground truth, \mathcal{I} . The final loss is then given by:

$$\mathcal{L} = \mathcal{L}_{\text{dcGAN}}(\mathcal{G}, \mathcal{D}) + \alpha \mathbb{E}_{x \sim p(\mathcal{X})} [\mathcal{L}_{cr}(\mathcal{O}, \mathcal{G}(x, \mathcal{E}(x)))] \quad (9)$$

where, \mathcal{L}_1 is the standard per-pixel loss, $x \sim p(\mathcal{X})$ is the input morph and \mathcal{E} is the image encoder. Throughout our experiments, we set $\alpha=1$.

Table 1. Dataset statistics after preprocessing. ‘L’ refers to landmark based morphs, while ‘D’ indicates deep-learning based morphs.

Dataset	Type	No. of train morphs	No. of test morphs	No. of train subjects	No. of test subjects
AMSL	L	823	302	56	33
StyleGAN	D	480	161	60	38
WebMorph	L	480	160	60	37
FaceMorpher	L	249	100	55	31
MorDiff	D	195	62	43	26
OpenCV	L	474	160	60	37

3.2. Implementation details

Demorphing: Our pipeline consists of three components: i) an image encoder \mathcal{E} , ii) a generator \mathcal{G} , and iii) a discriminator \mathcal{D} . For \mathcal{E} , we use a CLIP-based [30] image encoder to effectively process and represent facial information. The choice of CLIP over face-specific models is due to its general-purpose utility. Since morphs often contain high-frequency artefacts and overlapping features, a general-purpose encoder like CLIP is more robust and offers better representation than models trained solely on real faces. We use CLIP-ViT-B/32 model as a morph encoder which is based on the transformer architecture. The 32 in ViT-B/32 refers to the size of the image patches. In this model, each image is divided into 32×32 pixel patches. These patches are then linearly embedded into a sequence of tokens that are processed by the transformer layers. We use a pretrained CLIP model from the HuggingFace library, which produces embeddings of size 1×512 . We repeat the embedding 77 times, mimicking the practice used in Stable Diffusion [32]. For the generator, we use HuggingFace implementation of conditional UNet, namely, UNet2DConditionModel featuring 6 ResNet downsampling blocks and an equal number of ResNet upsampling blocks. Self-attention is implemented in the fifth downsampling block and the second upsampling block, allowing the model to focus on important spatial features. Along with the image, the UNet also receives morph embeddings, which are injected into intermediate layers of both the downsampling and upsampling blocks. This integration allows the outputs to retain context about the original morph image throughout the generation process. This UNet implementation also requires a timestep, which we have consistently set to zero in all our experiments, effectively eliminating its impact. Finally, our Discriminator is based on a CNN architecture consisting of four blocks, each containing a convolutional layer, InstanceNorm [40], and LeakyReLU. The discriminator concatenates the real and synthetic triplets along the channel axis and outputs a real/synthetic score.

Face Recognition Models and Parameters: We thoroughly evaluate our demorphing method using five publicly available Face Recognition Models: AdaFace [20],

ArcFace [11], VGG-Face [26], FaceNet [35], and OpenFace [3]. We evaluate the performance of each FRS in the presence of high-frequency artefacts introduced during the generation process. While we benchmark five different FRS, we use ArcFace as the primary FRS, consistent with its use in [5]. Each FRS is employed with its default settings as provided by the authors. We use cosine similarity to compute the biometric match score. Training is conducted using Adam optimization [21] with multi-GPU support via accelerate [16]. The training parameters are as follows: number of epochs: 300, learning rate: 10^{-4} , dropout rate=0.1, $\beta_1=0.5$ and $\beta_2=0.999$.

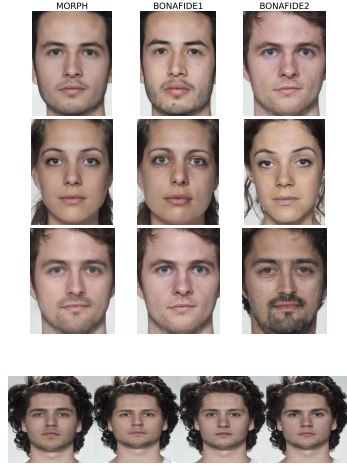


Figure 2. (Top) Challenging samples in the AMSL-Morph dataset: Typically, morphs are created by overlaying a face image onto a *base* image. These morphs are nearly indistinguishable from the base image, providing minimal information to the demorphing algorithm about the second image hindering the generation. (Bottom) Morphs created from same *base* image.

Table 2. Intrinsic bias in morphs towards the *base* image: We calculate the shift between MORPH-BF1 and MORPH-BF2 similarities and determine the d' value. The morph images are biometrically closer to the *base*-image than to the other image, making its recovery challenging.

	AdaFace	ArcFace	VGG-Face	Facenet	OpenFace
AMSL	2.26	1.39	1.42	1.15	1.71
OpenCV	1.20	1.49	1.51	1.27	1.39
FaceMorpher	1.35	1.59	1.43	1.32	1.41
WebMorph	1.05	1.29	1.41	1.15	1.48
MorDiff	1.05	1.29	1.34	1.30	1.73
StyleGAN	1.07	1.39	1.16	1.51	2.04

4. Dataset and Preprocessing

We conduct our experiments on three well-known morph datasets: AMSL [24], FRLL-Morphs [10], and MorDiff [7]. The FRLL-Morphs dataset includes morphs gener-

ated using four different techniques: OpenCV [22], StyleGAN [19], WebMorph [9], and FaceMorph [29]. In all three datasets, the bonafides are derived from the FRLL dataset, which comprises 102 identities, each with two frontal images (one smiling and one neutral). The morph counts in each of the dataset are as follows: AMSL: 2,175 morphs; FaceMorpher: 1,222 morphs; StyleGAN: 1,222 morphs; OpenCV: 1,221 morphs; WebMorph: 1,221 morphs; MorDiff: 1,000 morphs.

To split the dataset into training and testing sets, we follow an identity-disjoint protocol. We divide the 102 identities into training and testing sets using a 60-40 split. A morph image is included in the training (or test) set only if both bonafide identities used to create it belong to the training (or test) set. Morphs where one identity belongs to the training set and the other to the test set (or vice versa) are excluded. Additionally, any identities that do not participate in morph generation are also discarded. To maintain consistency across datasets, we only consider neutral faces (AMSL morphs are exclusively generated from neutral facial expressions bonafides).

Intrinsic Bias in Morphs: Figure 2 shows randomly selected examples from the AMSL dataset. Typically, a morph is created by superimposing a face image onto a *base image*. This process inherently introduces a bias toward the *base image*, making it extremely difficult to recover the other identity from the morph. To quantify this bias, we compute the similarity distributions between the morph and the two ground-truth images (MORPH-BF1 and MORPH-BF2) and calculate the d' values for each in Table 2. A higher d' value indicates that the distributions are well separated. This method of creating morphs leaves very little visual information about the second identity, making it extremely challenging to reconstruct it accurately. As a result, the outputs often closely resemble the morph itself, a phenomenon we refer to as *morph-replication*.

Preprocessing: All images are processed using MTCNN [42] to detect faces, after which they are cropped to include only the face regions. The images are then normalized and resized to a resolution of 256×256 . We discard the images on which faces cannot be detected. Importantly, no additional spatial transformations are applied to the images. This ensures that the facial features (such as lips, nose, etc.) of both morphs and ground-truth constituent images remain aligned during training. We present the dataset statistics in Table 1.

5. Experimental Analysis

5.1. Evaluation Criteria

Given a morphed face image MORPH as input, our reference-free method generates two output images, OUT1 and OUT2. Since the outputs are unordered, we deter-



Figure 3. To simulate real-world variations, we apply random transformations to the reference image. It’s important to note that these transformations are not applied during the training phase.

mine the correct pairing with the ground truth face images, BF1 and BF2, by calculating the similarities for the two possible output-ground truth pairs. We use a face comparator \mathcal{B} to assess facial similarity. If the sum $\mathcal{B}(\text{BF1}, \text{OUT1}) + \mathcal{B}(\text{BF2}, \text{OUT2})$ is greater than $\mathcal{B}(\text{BF1}, \text{OUT2}) + \mathcal{B}(\text{BF2}, \text{OUT1})$, we deem (BF1, OUT1) and (BF2, OUT2) as the correct pairs; otherwise, we swap OUT1 with OUT2. For each OUT_i , we consider its correct pair BF_i as genuine, where $i, j \in \{1, 2\}$ without replacement. The imposter score is computed by identifying the closest matching face in the bonafide database, excluding the ground truth image.

Note that this evaluation strategy enables us to detect *morph-replication*. If our method replicates the MORPH as its outputs, i.e., $\mathcal{B}(\text{MORPH}, \text{OUT1}) \approx \mathcal{B}(\text{MORPH}, \text{OUT2})$, the similarity scores $\mathcal{B}(\text{BF1}, \text{OUT1}) + \mathcal{B}(\text{BF2}, \text{OUT2})$ will also be approximately equal to $\mathcal{B}(\text{BF1}, \text{OUT2}) + \mathcal{B}(\text{BF2}, \text{OUT1})$. As a result, the pairs (BF1, OUT1) and (BF2, OUT2) would be assigned arbitrarily, causing the match rate to drop close to zero. We evaluate our reference free demorphing method in terms of True Match Rate (TMR) at different thresholds of False Match Rate (FMR).

For differential demorphing, we use a modified approach. Given a MORPH and a reference image REF, our method generates an output image, OUT. We treat the ground-truth image BF and OUT as the genuine pair. For the imposter pair, we search the entire test set of bonafide images in the FRLL dataset and assign the face with the third highest similarity to OUT, excluding GT and REF for obvious reasons (hence third). During evaluation, we arbitrarily select one of the constituent face image used to create MORPH as the reference image. However, this does not reflect a real-world scenario, as the exact reference image used to create the morph might not be available during demorphing. To simulate this, we apply one or more random transformations to the reference image (see Figure 3), such as Gaussian blur, jitter, affine transformation, etc. It is important to note that these transformations were not applied during training.

5.2. Findings

We evaluate our method both visually and analytically. It is imperative for any demorphing method to produce visu-

Table 3. Reference Free Demorphing: We compute the True Match Rate (TMR in %) at various False Match Rate (FMR in %) thresholds (0.1/1/5/10) between the generated outputs (OUT1, OUT2) and the ground truth images (BF1, BF2) across the five FR models used. ArcFace performs most consistently across the FRS used in the presence of high-frequency artefacts (See Figure 4 and 5)

Dataset	TMR @ FMR \uparrow				
	AdaFace	ArcFace	VGGFace	FaceNet	OpenFace
	0.1/1.0/5.0/10.0	0.1/1.0/5.0/10.0	0.1/1.0/5.0/10.0	0.1/1.0/5.0/10.0	0.1/1.0/5.0/10.0
AMSL	17.75/42.91/46.93/56.83	0.0/83.76/91.81/ 93.86	0.0/18.25/28.50/43.34	0.0/23.22/29.52/43.86	1.02/5.34/9.04/13.65
OpenCV	5.7/15.82/41.77/51.58	0.0/0.0/90.51/ 93.99	0.0/0.0/31.01/50.63	0.0/0.0/24.68/54.71	2.53/4.11/14.56/21.52
StyleGAN	1.27/1.59/6.69/8.6	0.0/0.0/0.0/ 58.92	0.0/0.0/0.0/7.31	0.0/0.0/0.0/6.69	1.59/1.91/4.14/6.37
WebMorph	14.56/14.87/38.92/50.95	0.0/0.0/0.0/ 89.87	0.0/0.0/18.67/37.34	0.0/0.0/10.13/33.86	7.91/8.23/11.08/12.66
FaceMorpher	4.59/4.59/35.71/46.94	0.0/0.0/29.45.0/ 94.39	0.0/0.0/29.59/52.55	0.0/0.0/9.69/58.67	1.53/1.53/9.18/9.69
MorDiff	21.43/21.43/35.71/47.32	0.0/0.0/87.5/ 93.75	0.0/0.0/19.64/34.82	0.0/0.0/22.32/27.68	0.0/0.0/2.68/8.04

Table 4. Differential Demorphing: We compute the True Match Rate (TMR in %) at various False Match Rate (FMR in %) thresholds between the generated output (OUT) and the ground truth image (GT) across the five FR models used.

Dataset	TMR @ FMR \uparrow				
	AdaFace	ArcFace	VGGFace	FaceNet	OpenFace
	0.1/1.0/5.0/10.0	0.1/1.0/5.0/10.0	0.1/1.0/5.0/10.0	0.1/1.0/5.0/10.0	0.1/1.0/5.0/10.0
AMSL	14.47/16.98/20.75/30.82	86.88/87.50/88.75/ 94.88	13.12/15.00/22.50/35.75	7.50/11.88/24.38/32.50	8.75/11.88/13.75/16.25
OpenCV	46.54/55.97/62.89/71.70	73.12/76.88/83.12/ 88.12	23.12/23.75/34.38/39.38	32.50/32.50/46.25/57.50	6.25/10.62/18.12/21.88
StyleGAN	0.62/1.25/4.38/6.25	36.02/41.61/45.34/ 54.04	1.86/3.11/6.21/9.32	3.11/3.73/5.59/8.07	0.62/1.24/3.11/4.97
WebMorph	33.76/36.31/49.04/58.60	67.50/81.25/87.50/ 89.38	14.37/14.37/25.62/30.00	26.88/27.50/38.12/44.38	6.25/11.25/16.25/23.12
FaceMorph	79.00/79.00/94.00/ 98.00	94.00/94.00/95.00/97.40	34.00/34.00/53.00/58.00	60.00/60.00/68.00/75.00	9.00/9.00/23.00/26.00
MorDiff	73.77/73.77/77.05/81.97	85.48/85.48/88.71/ 90.32	40.32/40.32/40.32/43.55	35.48/35.48/46.77/54.84	17.74/17.74/20.97/27.42

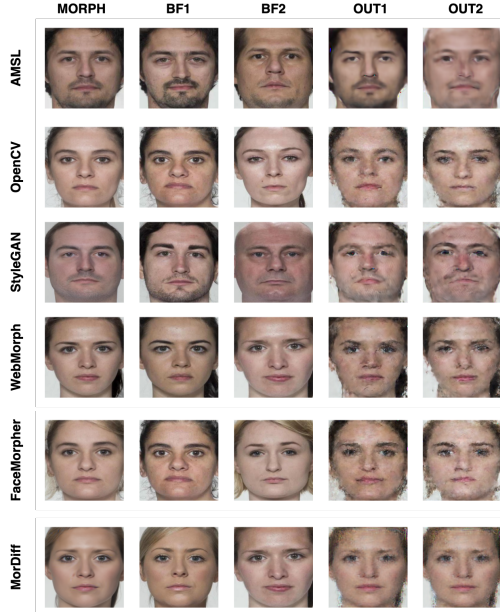


Figure 4. Reference-Free Demorphing Visualization: We illustrate the results of our reference-free demorphing approach. The model takes the morph image (MORPH) as input and produces two outputs (OUT1 and OUT2). The ground truth images used to generate the morph are denoted as BF1 and BF2.

ally distinctive faces compared to the input morph as well as between themselves. Note that a trivial solution for demor-

phing would be an identity function which simply outputs the morph. By construction, the outputs will have the best matches with the bonafide faces used to create the morph in the database, rendering the demorphing process unnecessary. Thus, visual evaluation is paramount in demonstrating the effectiveness of our method.

5.2.1 Reference Free Demorphing

We visualize the outputs of our reference-free demorphing method across six morphing techniques in Figure 4. These techniques include both landmark-based and deep-learning-based morphs. The first three columns visualize the morph and the two constituent face images used to create it, while the subsequent two columns show the outputs of our method, presented in no specific order. We observe that the faces produced by our method are visually distinct from each other and also appear notably different from the original morph. Moreover, they are visually closer to their ground-truth counterparts (refer to Appendix for more images). To quantify this, we calculate the normalized biometric distance between the generated faces and between the generated faces and the ground truth. We use five well-known face biometric models and plot the distance scores across three different pairings of images: OUT1-OUT2, BF1-OUT1, and BF2-OUT2, which represent the dissimilarity between the generated outputs and between each generated output and its corresponding ground truth. We plot the distance distribution for all datasets across all FR mod-

Table 5. Comparison of our reference-free approach to SDeMorph [38] and Identity-Preserving Demorphing (IPD) [39]. Unlike our method, which operates on unseen faces (scenario 3) and is significantly more challenging, the other methods assume the same identities are present in both training and test morphs (scenario 1). In scenario 3, our method significantly outperforms the current state-of-the-art method. The scores for scenario 3 are provided by the original authors of [38, 39].

Dataset	Ours (scenario 3)				SDeMorph (scenario 1)		SDeMorph (scenario 3)		IPD (scenario 1)		IPD (scenario 3)	
	AdaFace		ArcFace		AdaFace		ArcFace		AdaFace		AdaFace	
	Subject 1	Subject 2	Subject 1	Subject 2	Subject 1	Subject 2	Average		Subject 1	Subject 2	Average	
AMSL	8.60%	69.86%	85.43%	93.04%	97.70%	97.24%	12.56%		99.84%	99.56%	25.69%	
FaceMorpher	55.00%	43.00%	88.00%	93.00%	96.00%	99.50%	13.18%		-	-	37.82%	
MorDiff	70.96%	72.58%	83.87%	85.48%	78.00%	74.00%	11.67		-	-	38.12%	
StyleGAN	0.00%	0.00%	34.16%	47.82%	-	-	0.00%		-	-	16.22%	
WebMorph	22.20%	33.75%	85.62%	90.62%	-	-	12.80%		-	-	25.61%	

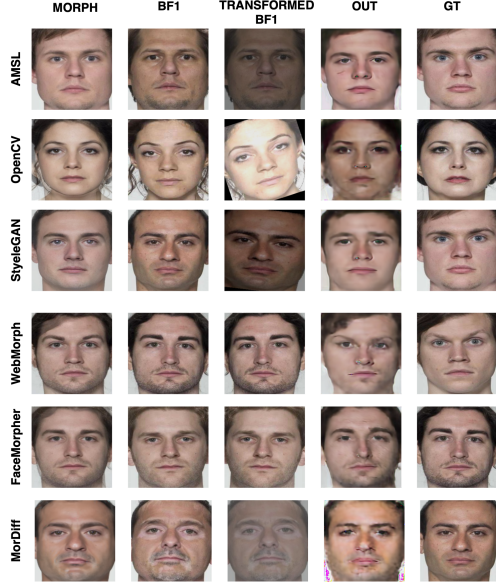


Figure 5. Differential Demorphing Visualization: We illustrate the results of our differential demorphing approach. The model receives the morph image (MORPH) and the transformed ground-truth image (TRANSFORMED BF1) and produces an output (OUT). The ground truth (GT) is shown, which, along with the ground-truth image (BF1), was used to generate the morph image (MORPH). Note that our method does not assume the demorphing process uses the exact same ground-truth image (BF1) that was used to create the morph.

Table 6. We compute image quality between generated face images and ground truth face images.

Method	FID↓	SSIM↑	LPIPS↓	PSNR↑
AMSL	0.3816	0.7765	0.2356	18.1377
OpenCV	0.1976	0.5742	0.2318	17.7306
FaceMorpher	0.5853	0.5554	0.2459	17.7578
WebMorph	0.2258	0.5696	0.2277	17.7022
StyleGAN	0.1506	0.5607	0.2520	18.3152
MorDiFF	1.0297	0.6631	0.2552	18.5223
Average	0.4284	0.6166	0.2414	18.0276

els in Figure 6. We observe an overall OUT1-OUT2 biometric distance of 0.4380, indicating a quantifiable difference in the output faces. Note that we use cosine distance rather than similarity to quantify results. This choice helps

us intuitively explain *morph-replication* because a greater distance indicates that the generated faces are more distinguishable from each other. For BF1-OUT1, we observe a distance of 0.3992, and for BF2-OUT2, a distance of 0.4025. Note that the distance scores between outputs and their respective ground-truth face images fall well below the threshold used in several biometric systems [36, 37]. Our method successfully learns to distinguish features from the base image, such as hair (Rows 1 and 3), skin color, and subtle details like eyebrows and facial hair. Finally, we compute the True Match Rate (TMR) of the output subjects at various False Match Rate (FMR) thresholds and present the results in Table 3. Our method achieves an average TMR of 93.86% on the AMSL dataset. The corresponding TMR values on the OpenCV, StyleGAN, WebMorph, FaceMorpher, and MorDiff datasets are 93.99%, 58.92%, 89.87%, 94.39%, and 93.75%, respectively. We also evaluate the quality of images generated by our method using various image-quality assessment (IQA) metrics, as shown in Table 6. Our method achieves an average FID [17] of 0.4284 across all datasets, with corresponding averages of 0.61 for SSIM [41], 0.24 for LPIPS [43], and 18.02 for PSNR, demonstrating the visual realism of the outputs from our method. We also observe that ArcFace performs consistently across all datasets in the presence of visual artefacts generated during demorphing compared to other FRS which is consistent with [5].

Comparison with SOTA: We evaluate our method against existing reference-free demorphing approaches based on restoration accuracy and TMR at 10% FMR. Restoration accuracy measures the proportion of outputs that correctly match their corresponding ground-truth images. Our method achieves an average TMR of 93.86% on the AMSL dataset using the ArcFace FRS, surpassing the performance of [5] by 23.32%. Reference-free demorphing methods, particularly for scenario 3, remain limited. Nonetheless, we also compare our method’s restoration accuracy with [38, 39] in both scenarios 1 and 3. In scenario 3, our method shows a significant performance advantage and achieves comparable results in scenario 1, despite being trained in the more challenging scenario 3. Results are summarized in Table 5.

Effect of \mathcal{L}_{cr} and $\mathcal{E}(\cdot)$: We conduct an ablation study on our method to assess i) the impact of cross-road loss and ii) the influence of dual conditioning on generation. Excluding pixel-wise guidance (the second part of the loss in Equation 9) results in an average performance decline of 20.87% across the six datasets tested on the ArcFace FRS. This decrease is mainly due to the model’s reduced ability to accurately align the two unordered generated outputs with the ordered ground-truth images. Moreover, when the generator is trained without \mathcal{E} , the performance drops by 8.57% due to lack of context during the generation (see Section 3). These results are presented in Table 9.

5.2.2 Differential demorphing

We visualize the results of differential demorphing in Figure 5. The first two columns show MORPH and BF1, the third column displays the randomly transformed BF1 used as the reference image in the demorphing process, and the remaining two columns present the output (OUT) from our method and the ground truth (GT). Our method produces faces that are visibly distinct from both the MORPH and the reference image achieving a TMR of 94.88% on the AMSL dataset, with corresponding values of 88.12%, 54.04%, 89.38%, 98.0%, and 90.32% on the OpenCV, StyleGAN, WebMorph, FaceMorph, and MorDiff datasets, respectively. These results are presented in Table 4.

Table 7. We calculate the average biometric distance for three cases —OUT1-OUT2, BF1-OUT1, and BF2-OUT2—across all five FR models utilized. (Individual scores in Appendix.)

Method	OUT1-OUT2 \uparrow	BF1-OUT1 \downarrow	BF2-OUT2 \downarrow
AMSL	0.4053	0.3324	0.3847
OpenCV	0.4910	0.4115	0.3878
FaceMorpher	0.4961	0.4084	0.4442
WebMorph	0.4825	0.3802	0.4078
StyleGAN	0.4193	0.4377	0.3864
MorDiff	0.3338	0.4247	0.4043
Average	0.4380	0.3992	0.4025

Table 8. We calculate the d' values for True versus Imposter scores in differential demorphing. Higher d' values suggest greater separability between the distributions.

	AdaFace	ArcFace	VGG-Face	FaceNet	OpenFace
AMSL	0.22	2.66	0.07	0.11	0.29
OpenCV	2.73	3.60	0.82	1.34	0.09
StyleGAN	1.39	0.80	1.17	1.02	0.99
WebMorph	0.93	2.07	0.10	0.27	0.15
FaceMorpher	1.49	2.04	0.35	0.50	0.33
MorDiff	2.02	1.96	0.62	0.45	0.17

6. Summary

In this paper, we propose dc-GAN, a novel method to recover facial identities from a morph. Our proposed method

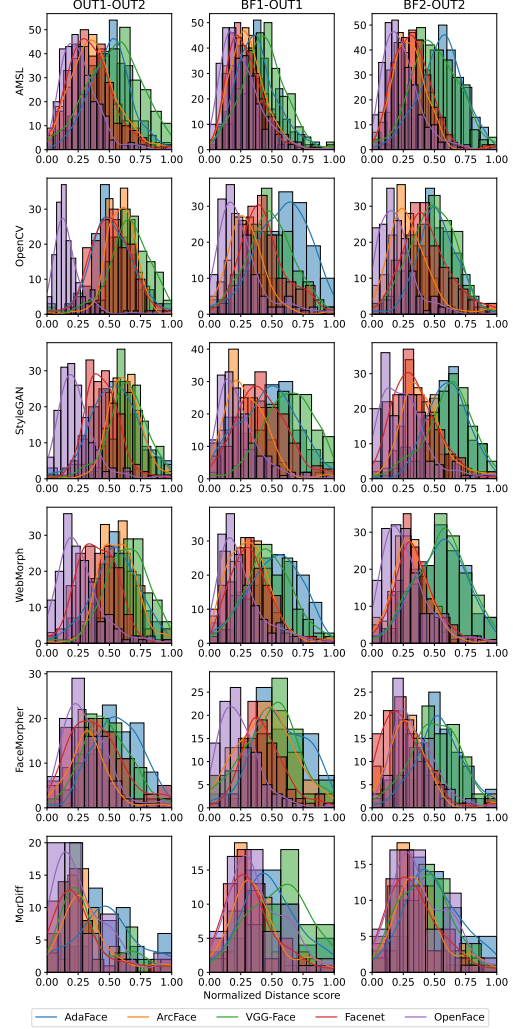


Figure 6. We plot the normalized distance scores for the pairs OUTPUT1-OUTPUT2, INPUT1-OUTPUT1, and INPUT2-OUTPUT2. Our method produces distinct face images, as illustrated in the left column.

Dataset	w/o \mathcal{L}_{cr}	w/o $\mathcal{E}(\cdot)$
AMSL	32.71/74.49/37.50/11.99/15.75	24.14/82.88/5.48/9.59/9.34
OpenCV	42.81/92.79/25.49/27.12/15.03	57.86/86.65/29.56/13.52/15.03
StyleGAN	9.03/56.13/7.42/7.74/12.58	6.25/52.5/6.25/9.38/3.75
WebMorph	39.69/84.38/28.75/29.69/17.19	36.25/79.69/25.31/16.56/10.0
FaceMorpher	43.03/91.30/26.77/19.19/22.73	50.00/90.04/32.83/25.25/9.60
MorDiff	37.29/0.0/1.69/3.39/15.25	48.86/81.25/40.18/24.11/21.43

Table 9. Effect of the dual-condition and \mathcal{L}_{cr} across five FRS used (AdaFace/ArcFace/VGG-Face/FaceNet/OpenFace). The drop in TMR performance shows the importance of the pixel-wise guidance during training and the effectiveness of the condition by \mathcal{E} during generation.

is based on GAN architecture, we condition our GAN on morphs as well as their latent representation to provide robust guidance while recovering identities. Previous ap-

proaches suffered from *morph-replication*, i.e., they produced similar-looking faces. Our method overcomes this problem significantly. We evaluate our method on 6 different morphing techniques using five biometric face models. We assessed our method using the AMSL, FRLL-Morphs, and MorDiff datasets, achieving visually compelling results and addressing the issue of *morph-replication*. Moreover, experiments suggest that ArcFace performs most consistently for demorphing tasks. Future work will aim to develop techniques for demorphing faces in various styles, beyond just passport-style face images.

References

- [1] Gnu image manipulation program (gimp), 2016. 1
- [2] P. Aghdaie, B. Chaudhary, S. Soleymani, J. Dawson, and N. M. Nasrabadi. Morph detection enhanced by structured group sparsity. In *IEEE/CVF Winter Conference on Applications of Computer Vision Workshops (WACVW)*. IEEE Computer Society, 2022. 1
- [3] Brandon Amos, Bartosz Ludwiczuk, and Mahadev Satyanarayanan. Openface: A general-purpose face recognition library with mobile applications. Technical report, CMU-CS-16-118, CMU School of Computer Science, 2016. 4
- [4] André Anjos and Sébastien Marcel. Counter-measures to photo attacks in face recognition: A public database and a baseline. In *International Joint Conference on Biometrics (IJCB)*, pages 1–7, 2011. 1
- [5] Sudipta Banerjee, Prateek Jaiswal, and Arun Ross. Facial de-morphing: Extracting component faces from a single morph. In *IEEE International Joint Conference on Biometrics (IJCB)*. IEEE, 2022. 1, 2, 3, 4, 7
- [6] Sudipta Banerjee and Arun Ross. Conditional identity disentanglement for differential face morph detection. In *2021 IEEE International Joint Conference on Biometrics (IJCB)*, pages 1–8, 2021. 2
- [7] Naser Damer, Meiling Fang, Patrick Siebke, Jan Niklas Kolf, Marco Huber, and Fadi Boutros. Mordiff: Recognition vulnerability and attack detectability of face morphing attacks created by diffusion autoencoders. In *11th International Workshop on Biometrics and Forensics (IWBF)*, pages 1–6, 2023. 1, 4
- [8] Naser Damer, César Augusto Fontanillo López, Meiling Fang, Noémie Spiller, Minh Vu Pham, and Fadi Boutros. Privacy-friendly synthetic data for the development of face morphing attack detectors. In *Proceedings of the IEEE/CVF Conference on Computer Vision and Pattern Recognition*, 2022. 1
- [9] Lisa DeBruine. `debruine/webmorph`: Beta release 2, Jan. 2018. 5
- [10] Lisa DeBruine and Benedict Jones. Face research lab london set, May 2017. 4
- [11] Jiankang Deng, Jia Guo, Niannan Xue, and Stefanos Zafeiriou. Arcface: Additive angular margin loss for deep face recognition. In *Proceedings of the IEEE/CVF Conference on Computer Vision and Pattern Recognition*, pages 4690–4699, 2019. 4
- [12] Zeev Farbman, Raanan Fattal, Dani Lischinski, and Richard Szeliski. Edge-preserving decompositions for multi-scale tone and detail manipulation. *ACM Trans. Graph.*, 2008. 1
- [13] Matteo Ferrara, Annalisa Franco, and Davide Maltoni. Face demorphing. *IEEE Transactions on Information Forensics and Security*, 2018. 1, 2
- [14] Matteo Ferrara, Annalisa Franco, and Davide Maltoni. Decoupling texture blending and shape warping in face morphing. In *International Conference of the Biometrics Special Interest Group (BIOSIG)*, pages 1–5, 2019. 1
- [15] Ian J. Goodfellow, Jean Pouget-Abadie, Mehdi Mirza, Bing Xu, David Warde-Farley, Sherjil Ozair, Aaron Courville, and Yoshua Bengio. Generative adversarial nets. In *Proceedings of the 27th International Conference on Neural Information Processing Systems - Volume 2, NIPS*. MIT Press, 2014. 3
- [16] Sylvain Gugger, Lysandre Debut, Thomas Wolf, Philipp Schmid, Zachary Mueller, Sourab Mangrulkar, Marc Sun, and Benjamin Bossan. Accelerate: Training and inference at scale made simple, efficient and adaptable. <https://github.com/huggingface/accelerate>, 2022. 4
- [17] Martin Heusel, Hubert Ramsauer, Thomas Unterthiner, Bernhard Nessler, and Sepp Hochreiter. Gans trained by a two time-scale update rule converge to a local nash equilibrium. In *Proceedings of the 31st International Conference on Neural Information Processing Systems, NIPS’17*, page 6629–6640, Red Hook, NY, USA, 2017. Curran Associates Inc. 7
- [18] Phillip Isola, Jun-Yan Zhu, Tinghui Zhou, and Alexei A Efros. Image-to-image translation with conditional adversarial networks. *CVPR*, 2017. 3
- [19] Tero Karras, Samuli Laine, Miika Aittala, Janne Hellsten, Jaakko Lehtinen, and Timo Aila. Analyzing and improving the image quality of StyleGAN. In *Proc. CVPR*, 2020. 5
- [20] Minchul Kim, Anil K Jain, and Xiaoming Liu. Adaface: Quality adaptive margin for face recognition. In *Proceedings of the IEEE/CVF conference on computer vision and pattern recognition*, 2022. 4
- [21] Diederik P. Kingma and Jimmy Ba. Adam: A method for stochastic optimization. In Yoshua Bengio and Yann LeCun, editors, *3rd International Conference on Learning Representations, ICLR*, 2015. 4
- [22] Satya Mallick. Face morph using `opencv—c++/python`. *LearnOpenCV*, 1(1), 2016. 5
- [23] Matthias Monroy. Laws against morphing, 2020. 1
- [24] Tom Neubert, Andrey Makrushin, Mario Hildebrandt, Christian Kraetzer, and Jana Dittmann. Extended stirtrace benchmarking of biometric and forensic qualities of morphed face images. *IET Biometrics*, 2018. 4
- [25] Mei Ngan, Patrick Grother, Kayee Hanaoka, and Jason Kuo. Face recognition vendor test (frvt) part 4: Morph - performance of automated face morph detection, 2020-03-06 2020. 1
- [26] Omkar M. Parkhi, Andrea Vedaldi, and Andrew Zisserman. Deep face recognition. In *The British Machine Vision Conference*, 2015. 4

- [27] Deepak Pathak, Philipp Krähenbühl, Jeff Donahue, Trevor Darrell, and Alexei Efros. Context encoders: Feature learning by inpainting. 2016. 3
- [28] Fei Peng, Le-Bing Zhang, and Min Long. Fd-gan: Face de-morphing generative adversarial network for restoring accomplice’s facial image. *IEEE Access*, 2019. 2
- [29] A Quek. Face morpher. 5
- [30] Alec Radford, Jong Wook Kim, Chris Hallacy, Aditya Ramesh, Gabriel Goh, Sandhini Agarwal, Girish Sastry, Amanda Askell, Pamela Mishkin, Jack Clark, Gretchen Krueger, and Ilya Sutskever. Learning transferable visual models from natural language supervision. In *International Conference on Machine Learning*, 2021. 4
- [31] R. Raghavendra, Kiran B. Raja, and Christoph Busch. Detecting morphed face images. In *IEEE 8th International Conference on Biometrics Theory, Applications and Systems (BTAS)*, 2016. 1
- [32] Robin Rombach, Andreas Blattmann, Dominik Lorenz, Patrick Esser, and Björn Ommer. High-resolution image synthesis with latent diffusion models. In *Proceedings of the IEEE/CVF Conference on Computer Vision and Pattern Recognition (CVPR)*, 2022. 4
- [33] Olaf Ronneberger, Philipp Fischer, and Thomas Brox. U-net: Convolutional networks for biomedical image segmentation. In *Medical image computing and computer-assisted intervention—MICCAI*, 2015. 3
- [34] Ulrich Scherhag, Dhanesh Budhrani, Marta Gomez-Barrero, and Christoph Busch. Detecting morphed face images using facial landmarks. In Alamin Mansouri, Abderrahim El Moataz, Fathallah Nouboud, and Driss Mammass, editors, *Image and Signal Processing*, Cham, 2018. Springer International Publishing. 1
- [35] Florian Schroff, Dmitry Kalenichenko, and James Philbin. Facenet: A unified embedding for face recognition and clustering. In *Proceedings of the IEEE Conference on Computer Vision and Pattern Recognition (CVPR)*, June 2015. 4
- [36] Sefik Serengil and Alper Ozpinar. A benchmark of facial recognition pipelines and co-usability performances of modules. *Journal of Information Technologies*, 17(2):95–107, 2024. 7
- [37] Sefik Ilkin Serengil and Alper Ozpinar. Lightface: A hybrid deep face recognition framework. In *2020 Innovations in Intelligent Systems and Applications Conference (ASYU)*, pages 23–27. IEEE, 2020. 7
- [38] Nitish Shukla. Sdemorph: Towards better facial demorphing from single morph. In *IEEE International Joint Conference on Biometrics (IJCB)*. IEEE, 2023. 1, 2, 7
- [39] Nitish Shukla and Arun Ross. Facial demorphing via identity preserving image decomposition. *IEEE International Joint Conference on Biometrics (IJCB)*, 2024. 2, 7
- [40] Dmitry Ulyanov, Andrea Vedaldi, and Victor S. Lempitsky. Instance normalization: The missing ingredient for fast stylization. *ArXiv*, abs/1607.08022, 2016. 4
- [41] Zhou Wang, A.C. Bovik, H.R. Sheikh, and E.P. Simoncelli. Image quality assessment: from error visibility to structural similarity. *IEEE Transactions on Image Processing*, 13(4):600–612, 2004. 7
- [42] K. Zhang, Z. Zhang, Z. Li, and Y. Qiao. Joint face detection and alignment using multitask cascaded convolutional networks. *IEEE Signal Processing Letters*, 23(10):1499–1503, Oct 2016. 5
- [43] Richard Zhang, Phillip Isola, Alexei A Efros, Eli Shechtman, and Oliver Wang. The unreasonable effectiveness of deep features as a perceptual metric. In *Proceedings of the IEEE Conference on Computer Vision and Pattern Recognition (CVPR)*, 2018. 7

Supplementary Material for “dc-GAN: Dual-Conditioned GAN for Face Demorphing From a Single Morph”

Anonymous WACV Algorithms Track submission

Paper ID *****

1. Reconstructions

We vizualize images produced by our method on six datasets in Figure 1, 2, 3, 4, 5 and 6. The first row vizualizes the morph image, subsequent two rows are the outputs from our method and next two rows are the ground-truth images.



Figure 1. AMSL



Figure 2. OpenCV



Figure 3. StyleGAN



Figure 5. FaceMorpher



Figure 4. WebMorph



Figure 6. MorDiff

2. Results

2.1. Reference Free Demorphing: Individual Biometric Distance Scores

For reference free demorphing, we calculate biometric distance scores across three cases: i) OUT1-OUT2, which measures the distinction between the two outputs of our method; ii) BF1-OUT1, which assesses how closely the first output matches its corresponding ground truth; and iii) BF2-OUT2, which assesses the similarity of the second output to its respective ground truth.

Table 1. Biometric Distance Score across three cases.

Dataset	Model	OUT1-OUT2	BF1-OUT1	BF2-OUT2
AMSL	AdaFace	0.502	0.376	0.538
	ArcFace	0.349	0.262	0.521
	VGG-Face	0.593	0.376	0.653
	Facenet	0.349	0.262	0.521
	OpenFace	0.562	0.336	0.477
StyleGAN	AdaFace	0.549	0.566	0.635
	ArcFace	0.402	0.261	0.342
	VGG-Face	0.563	0.337	0.478
	Facenet	0.399	0.320	0.234
	OpenFace	0.277	0.381	0.385
WebMorph	AdaFace	0.482	0.426	0.546
	ArcFace	0.342	0.278	0.502
	VGG-Face	0.589	0.318	0.547
	Facenet	0.462	0.347	0.491
	OpenFace	0.551	0.295	0.323
FaceMorpher	AdaFace	0.373	0.422	0.482
	ArcFace	0.336	0.411	0.478
	VGG-Face	0.420	0.251	0.555
	Facenet	0.354	0.357	0.396
	OpenFace	0.469	0.295	0.365
OpenCV	AdaFace	0.502	0.376	0.538
	ArcFace	0.349	0.262	0.521
	VGG-Face	0.593	0.376	0.653
	Facenet	0.349	0.262	0.521
	OpenFace	0.562	0.336	0.477
MorDiff	AdaFace	0.549	0.566	0.635
	ArcFace	0.402	0.261	0.342
	VGG-Face	0.563	0.337	0.478
	Facenet	0.399	0.320	0.234
	OpenFace	0.277	0.381	0.385

2.2. Differential Demorphing: True vs Imposter scores

For differential demorphing, we compute the distribution of true scores which is defines as biometric similarity between the output and ground-truth image. We also calculate the imposter score which is the biometric similarity of our output to the third best closest image in FRLL dataset. We plot these distributions across five FR model in Figure 7.

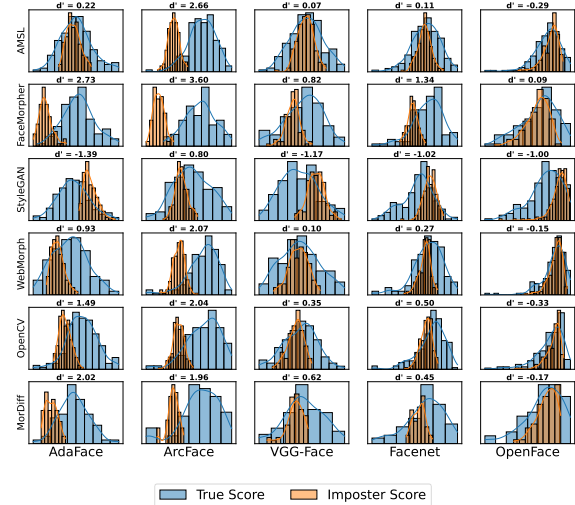


Figure 7. We present the true-imposter similarity scores for differential demorphing. For each plot, the d' value is indicated, which measures the separation between the true and imposter distributions.

3. Intrinsic bias in Morphs

We calculate the biometric similarity between morphs and the constituent images used to create them, then plot these distributions across five FR models in Figure 8. The blue distribution represents the similarity between the MORPH image and the first constituent image (BF1), while the orange curve shows the similarity between the MORPH image and the second constituent image (BF2). The separation between these two curves, as quantified by their d' value, illustrates the bias introduced by the morphing process.

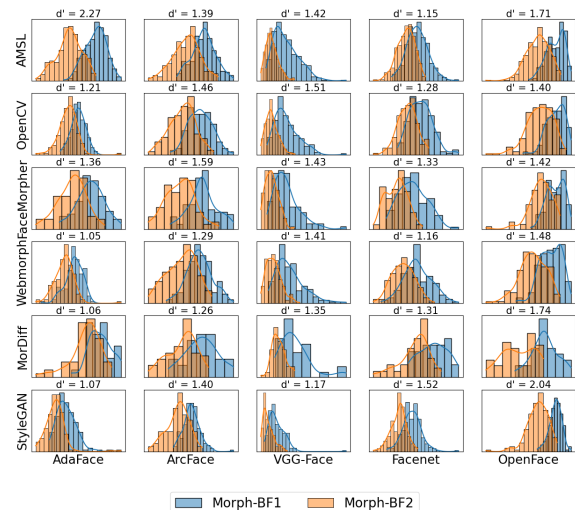


Figure 8. Intrinsic bias in producing morphs: We plot the normalized similarity score of MORPH-BF1 and MORPH-BF2.

Table 2. Generalization across morph techniques: We train our method on AMSL and evaluate on remaining datasets. We compute the True Match rate (TMR) at various False Match rate (FMR) thresholds across the five FRS systems used.

Dataset	Subject	TMR @ %FMR				
		AdaFace	ArcFace	VGGFace	FaceNet	OpenFace
		0.1/1.0/5.0/10.0	0.1/1.0/5.0/10.0	0.1/1.0/5.0/10.0	0.1/1.0/5.0/10.0	0.1/1.0/5.0/10.0
OpenCV	Subject1	28.77/39.04/67.47/75.0	4.07/8.47/23.39/43.05	3.69/13.42/25.5/41.28	2.36/5.72/27.61/36.36	3.03/7.07/21.21/31.99
	Subject2	0.0/0.0/3.42/8.56	0.34/0.68/8.14/12.54	0.67/1.34/14.77/20.81	1.68/3.37/15.49/21.21	2.02/5.05/11.11/18.52
StyleGAN	Subject1	37.68/47.89/62.32/70.42	3.77/7.41/32.66/44.11	5.05/15.49/32.66/42.76	2.35/4.7/29.53/37.25	0.34/5.41/23.31/33.78
	Subject2	0.0/0.0/5.99/9.86	0.0/0.34/7.41/13.13	1.01/4.38/12.12/23.23	1.34/1.68/14.09/21.48	2.03/5.74/12.16/19.93
WebMorph	Subject1	32.51/45.58/57.6/70.32	3.69/12.08/32.21/45.97	2.0/9.0/27.33/35.0	8.67/11.67/29.67/38.67	3.67/5.67/25.0/37.67
	Subject2	0.35/1.41/2.83/7.77	1.01/1.01/8.05/17.11	0.67/4.0/9.67/22.0	4.0/4.0/11.33/24.0	0.33/3.67/13.33/23.33
FaceMorph	Subject1	31.83/39.45/56.06/76.12	7.0/14.67/27.33/43.33	2.33/10.33/30.33/38.33	4.0/8.33/33.0/40.67	1.33/3.0/20.0/33.0
	Subject2	0.0/0.35/5.54/11.07	0.67/1.67/9.67/15.0	0.33/3.33/9.0/23.33	0.67/4.33/19.33/27.0	2.33/4.33/12.0/22.67
MorDiff	Subject1	29.51/46.88/61.81/76.04	10.33/14.0/30.67/46.33	4.0/12.33/23.33/37.67	4.33/5.33/27.0/42.33	0.67/7.33/18.33/27.67
	Subject2	0.0/0.0/2.78/10.42	1.0/2.33/9.33/14.0	1.33/5.67/9.67/26.67	1.33/4.67/12.0/18.0	1.67/3.33/11.33/22.33

4. Inter-Dataset Generalizability

We evaluate our method’s ability to generalize across different morphing techniques by training it on the AMSL dataset and assessing its performance on other datasets. Visual results are shown in Figure 9. Our method demonstrates strong generalization regardless of the morphing procedure applied. Additionally, we calculate the True Match Rate (TMR) across various False Match Rates (FMR), as presented in Table 2.

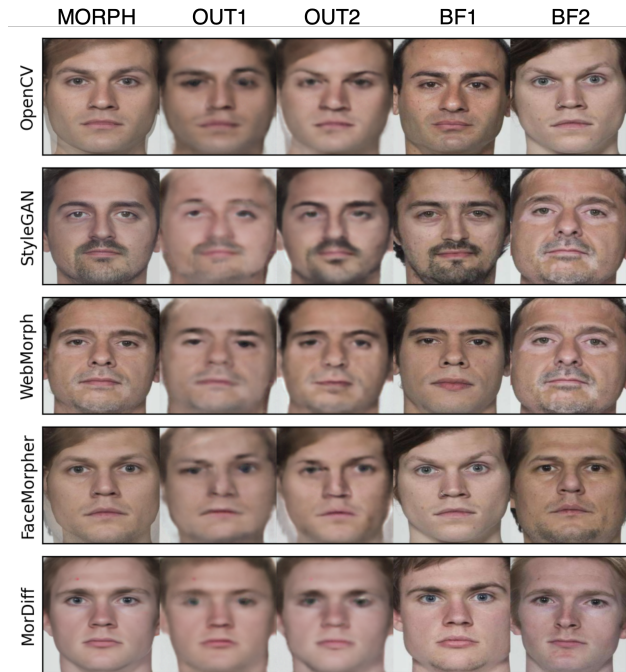


Figure 9. Generalizability of our demorphing method: We trained our method on the AMSL dataset and tested it on the remaining datasets, demonstrating strong generalization across different morph techniques."